Geomechanics and Engineering, *Vol. 31, No. 6 (2022) 557-571*
https://doi.org/10.12989/gae.2022.31.6.557

Mechanical properties of tailings with dipping interlayers under high confining pressure

Qinglin Chen[1,2a], Zugui Li[1,2b], Zeyu Dai[1,2c], Xiaojun Wang[1,2d] and Chao Zhang*[1,2]

[1]*School of Resources and Environmental Engineering, Jiangxi University of Science and Technology, Ganzhou, Jiangxi 341000, China*
[2]*State Key Laboratory of Geomechanics and Geotechnical Engineering, Institute of Rock and Soil Mechanics, Chinese Academy of Sciences, Wuhan, Hubei 430071, China*

(*Received November 23, 2021, Revised October 11, 2022, Accepted December 2, 2022*)

Abstract. Landslides are often triggered by weak interlayers initiated in tailings dam foundations, and hazards gradually occur. This is serious for landslides in high tailings dams due to their high potential energy. Tailing samples with a fine-grained interlayer at a set dip angle were prepared. Consolidated undrained (CU) triaxial shear tests were carried out by using a high-pressure triaxial apparatus. The results were compared with the results under a low confining pressure. Four reasons were summarized for high tailings dams more prone to instability than low dams. The shear strength of the samples with dipping interlayers decreases with increasing dip angle. An obvious straight drop in the stress path after the peak occurs in samples with dipping interlayers at an angle of 60°. The effect of the interlayer on the mechanical behaviour of tailings is very sensitive, especially for the sample with a dipping interlayer at an angle of 60°. Shear slipping along the interlayer should be given more attention in tailings dams. Compared with the results under low confining pressure, the stress decreases continuously for the samples with dipping interlayers at large angles under high confining pressure. The positive pore pressure, which reduces the effective stress, occurred in tailings samples under high confining pressure. The residual strength of tailings under high confining pressure is smaller than that under low confining pressure. These factors increase the dam break risk and the disaster impact for high tailings dams.

Keywords: critical state; deformation patterns; fine-grained interlayer; high confining pressure; tailings

1. Introduction

In the mining industry, tailings are the remains of various ore wastes produced during the mining process (Dong *et al.* 2020). Since 2012, annual mineral resource extraction has exceeded 10 billion tons in China. The total production of nonferrous metals and iron ore has increased by an average of more than 2 billion tons per year. Meanwhile, 1.6 billion tons of tailings are generated per year. The underground backfilling and the surface disposal methods are used to dispose of the tailings (Jiang *et al.* 2020, Xue *et al.* 2022). The underground backfilling method is that the tailings are filled to underground goaf (Kou *et al.* 2020). It not only ensures the safely extract ore from stopes, but also disposes of the tailings. The backfilling is becoming increasingly important as a result of the trends in mining to mine deeper (Cao *et al.* 2020, Cao *et al.* 2021). The surface disposal method is that tailings ponds were constructed to dispose of the tailings. More than 12,000 tailings dams have been constructed in China *et al.* 2008), and more than 18,400 tailings dams have been constructed worldwide (Azam and Li 2010). In addition, to dipose of more tailings, the height of the tailings dams has increased in recent years (Ma *et al.* 2021). At present, there are at least 26 tailings dams with a height greater than 100 m and at least 10 tailings dams with a storage capacity of more than 100 million m^3 in China (Zhang *et al.* 2020). The Wanniangou tailings dam in Sichuan Province, China, is currently the highest tailings dam in the world. The height of this dam is 325 m, and the total storage capacity is 326 million m^3 (Li and Coop 2018). The tailings dam with the largest storage capacity in Asia is the Dexing tailings dam at No. 4. The height of the dam has exceeded 200 m, and its deposit was up to 890 million m^3 (Wu *et al.* 2016).

Tailings ponds with high potential energy are a potential source of debris flow. The accident hazard of tailings dams ranks 18th among 93 accident types in the world, behind only disasters such as nuclear explosions, nerve gas, and nuclear radiation (Komnitsas *et al.* 1998). Once the dam breaks, it poses a serious threat to downstream residents, industry and agriculture. In China, failures of tailings impoundments have resulted in the loss of many lives, considerable property damage, and irreversible contamination of downstream areas. From 2001 to 2012, a

∗Corresponding author, Professor
E-mail: 20172001004@cqu.edu.cn
[a]Ph.D.
E-mail: chenql@cqu.edu.cn
[b]Student
E-mail: 6720221232@mail.jxust.edu.cn
[c]Student
E-mail: 873748560@qq.com
[d]Ph.D.
E-mail: wangxiaojun@jxust.edu.cn

ISSN: 2005-307X (Print), 2092-6219 (Online)

total of 73 tailings dam failure accidents were reported, with more than 500 deaths in China. Among them, four dam failures were classified as major accidents. The safety of the tailings pond is getting worse (Koppe 2021). The International Commission on Large Dams (ICOLD) found that tailings pond accidents occurred mainly in four countries with rich mineral resources. The four countries are the United States, the United Kingdom, Chile and the Philippines. There were 22 major tailings dam failures in the United States, eight in Chile, six in the United Kingdom, and six in the Philippines (Krause 1997, Martin and McRoberts 1999, Campbell and Fitterman 2000, Jeyapalan 1982, Lottermoser and Ashley 2005, Achterberg *et al.* 1999, Davies and Martin 2000). For example, a failure of a tailings dam occurred in Shanxi Province, Northwest China, on August 10, 2008, causing 277 deaths (Yin *et al.* 2011). A failure of a tailings dam occurred in Brumadinho, Minas Gerais, southeastern Brazil, on January 25, 2019, causing at least 270 deaths (Cionek *et al.* 2019, Lumbroso *et al.* 2021).

The tailings dam is the most important part of the tailings pond. The safety of a tailings pond is directly affected by the stability of its dam. The tailings dams can be divided into upstream tailings dams, downstream tailings dams, centerline tailings dams, dry stacking tailings dams and reservoir tailings dams (Moolman and Vietti 2012, Farshad 2011, Wang *et al.* 2020). The first three types of dam construction techniques can be attributed to wet accumulation, which disposes of the tailings as slurry with high water content. Wet accumulation is currently a widely used method of dam construction, of which the upstream method is the most commonly used. Up to 95% of tailings dams use the upstream method of construction. After slurry tailings discharge to the tailings pond, tailings are settled under gravity. Generally, coarse tailings are settled faster than fine tailings. The distribution of tailings dams is coarse tailings in the upper beach and fine tailings in the ponds (Shao *et al.* 2021). However, due to the aggregation of fine particles during the sedimentation of the tailings, a layered or lens structure always appears (Özer and Bromwell 2012). Fig. 1 presents a sectional sketch of a tailings dam. The distribution of idealized tailings dams is different from that of actual tailings dams. Some lenticles were inserted in the actual tailings dam. The shear strength and permeability of fine-grained lenticle structures are poor (Jiang 2005). Therefore, the potential slip surface of tailings dams is prone to form in lenticle structures (Fan and Masliyah 1990, Blight 1994, Gomes *et al.* 2017).

At present, the effect of the interlayer on the mechanical properties of tailings has been studied under low confining pressure (Li *et al.* 2004). However, the weakening influence of the interlayer on the mechanical properties of tailings for high tailings dams is unclear. Moreover, due to the tailings dam with a slope angle, the direction of the principal stress is oblique to the distribution plane of the lenticle structures. The stress in the high dam is larger than that in the low dam. The risk of tailings dam failure increases with increasing stress. Therefore, the effect of the interlayer on the mechanical properties of tailings should be emphasized under high stress.

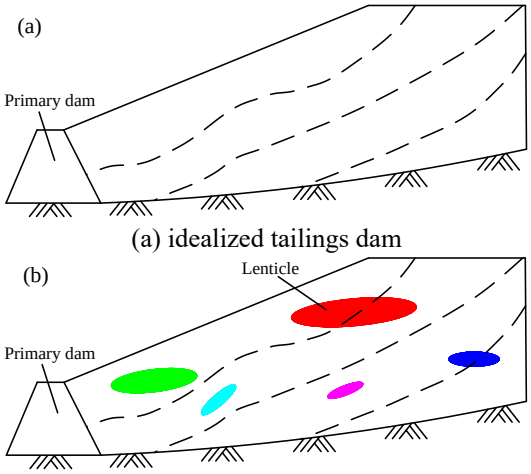

(a) idealized tailings dam

(b) actual tailings dam with lenticles

Fig. 1 Sectional sketch of tailings dam

The motivation for this paper is to study the strength and deformation of tailings with fine-grained interlayers under high confining pressure. Tailing samples with fine-grained interlayer at different dip angles prepared by an improved sample preparation method. Consolidated undrained (CU) triaxial shear tests were carried out by a high-pressure triaxial apparatus. The mechanical behaviour of tailings with interlayers at different dip angles was studied under high confining pressure. The results in this paper were compared with results under low confining pressure. The reasons were summarized for high tailings dams more prone to instability than low dams. Research results can provide a reference for the construction and long-term safe operation of the high tailings dams.

2. Material and methods

2.1 High-pressure triaxial apparatus

Fig. 2 presents the high pressure triaxial apparatus. The maximum confining pressure of the apparatus is 5 MPa, and the maximum back pressure is 1 MPa. The maximum stroke of the motor is 80 mm. The triaxial pressure chamber is made of stainless steel with a wall thickness of 12 mm. To study the mechanical behaviour of tailings with interlayers at different dip angles under high confining pressure, consolidated undrained (CU) tests were carried out.

2.2 Tailings materials

The tailings material belongs to a copper mine. The specific gravity is 2.6, and the moisture content is 11.65%. The mean particle size of the tailings was 0.14 mm. The mineral composition percentages of the tailings were determined by the reference intensity ratio (RIR) method. Quartz is the main mineral composition in tailings, with a percentage of 54.32%. Other mineralogical components are illite (38.38%), kaolinite (4.47%) and pyrite (2.83%), in descending order by content. Scanning electron microscopy (SEM) analysis was conducted to investigate the shape

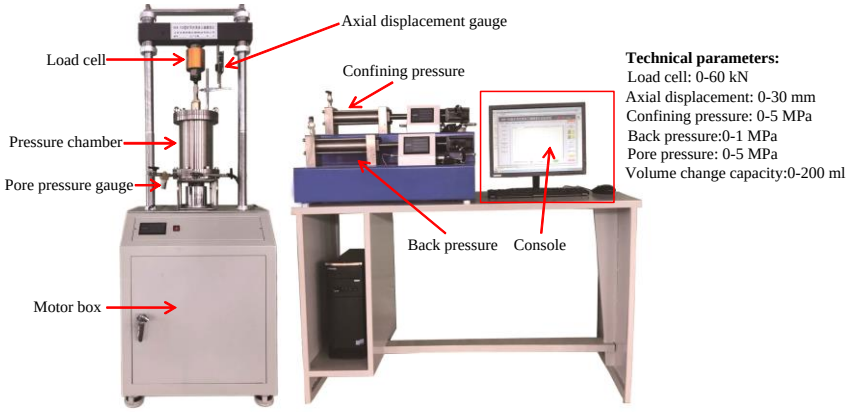

Fig. 2 Strain-controlled high pressure triaxial apparatus

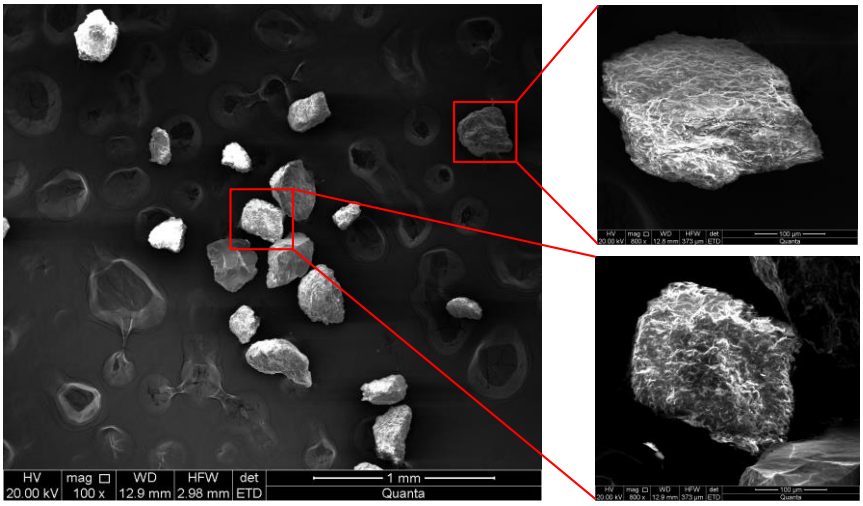

Fig. 3 Shape topography of tailing particles

topography of the tailings particles, as shown in Fig. 3. Tailing particles are angular. Their shape varies greatly. The ridge corners of some particles are sharp, and no unified profile can be found.

2.3 Sample preparation *and test program*

Fig. 4 presents the sample preparation method. First, half of the coarse tailings were poured into a sample tub of Φ 39.1 mm× L 140 mm. The coarse tailings were hammered tightly with tamping rods with angled end faces. Then, fine tailings were poured into the sample tub and flattened by the tamping rod to form the fine-grained interlayers. Finally, the remaining half of the coarse tailings were poured into the sample tub. The coarse tailings were compacted by the traditional tamping rod with a flat end face. Each interface of the layers was scratched with a knife. The height of the tailings samples was 80 mm when the two pistons of Φ 39.1 mm× L 30 mm were just emplaced into the sample tub. Tailing samples with a fine-grained interlayer at a set dip angle were prepared by the sample preparation method in this paper.

The diameter of all samples was 39.1 mm, and the height was 80 mm(Wood *et al.* 2008, Pan *et al*. 2020). The thickness of the interlayer is 5 mm for samples with dipping interlayers. The particle size inside the interlayer is smaller than 0.074 mm, and their dry density is 1.55 g/cm^3. The tailings outside the interlayer are unclassified coarse tailings, and their dry density is 1.75 g/cm3.

The dip angles of the specimens with interlayers are 0°, 15°, 30°, 45°, and 60°. The tested confining pressures are set to 1 MPa, 2 MPa, 3 MPa, and 4 MPa. The strain controls were carried out in this paper. The constant shear speed is 0.073 mm/min, according to the standard for soil test method (GB/T50123, 1999). When the axial strain reached 15%, the test ceased.

3. Experimental results

3.1 Stress-strain behaviour

Fig. 5 presents the stress-strain curves of tailings with dipping interlayers. The trend of the stress-strain curve is the same for samples with dipping interlayers at the same angle. The deviator stress at failure gradually increases as the confining pressure increases. The stress-strain curves are obviously affected by the dipping interlayer, especially

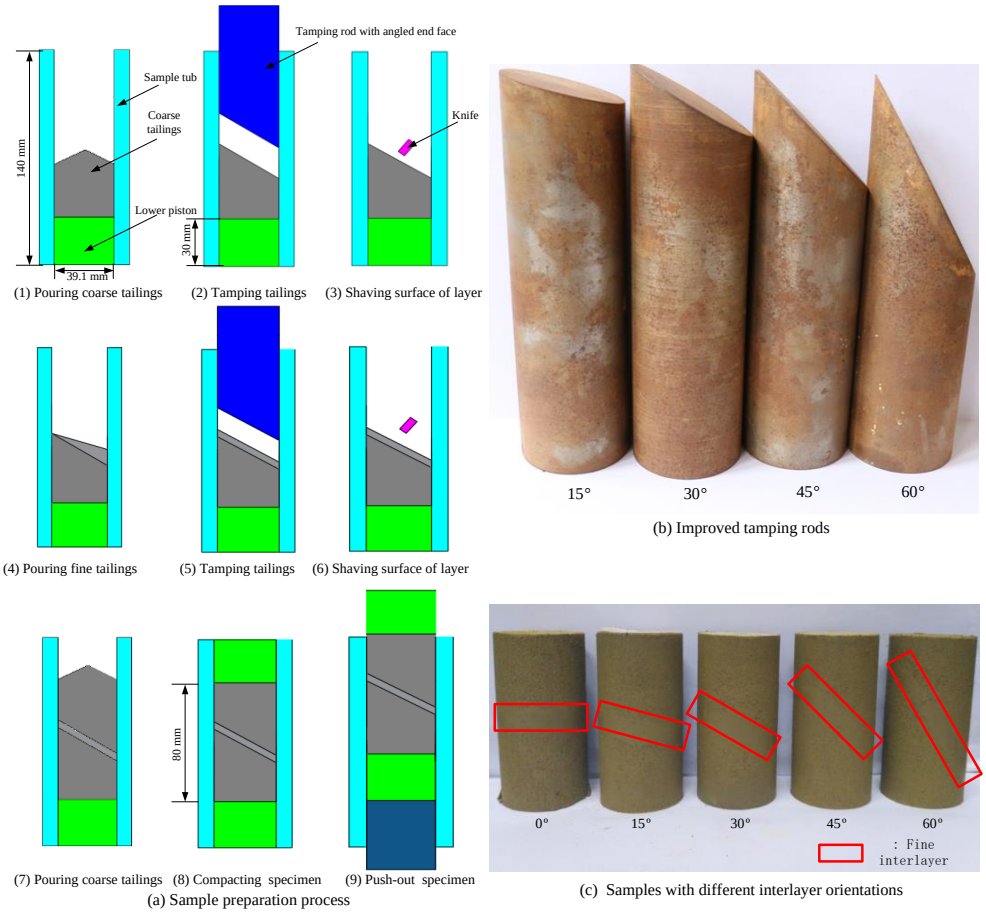

Fig. 4 Sample preparation method

for the sample with a dipping interlayer at an angle of 60°. Strain softening obviously occurs in the samples with dipping interlayers at an angle of 60°. The detailed results shown in these curves are as follows:

For the samples with a dipping interlayer at angles of 0°, 15°, and 30°, the deviator stress increases rapidly with the axial strain until the peak is reached, and then the deviator stress remains steady. The stress-strain behaviour is consistent with that of the coarse sample. When the confining pressure is large, the deviator stress shows a slight stress drop after the peak. This may be because the mechanical behaviour of the sample exhibited slight brittleness after consolidation under the large confining pressure.

For the samples with a dipping interlayer at an angle of 45°, the deviator stress of the samples under confining pressures of 1 MPa, 2 MPa, and 3 MPa remains steady after the peak. Strain softening occurs when the axial strain reaches 8% for the samples under a confining pressure of 4 MPa. The stress-strain behaviour is similar to that of the sample with a dipping interlayer at an angle of 60°. It indicates that strain softening is prone to occur when the dip angle of the interlayer is large.

For the samples with a dipping interlayer at an angle of 60°, the deviator stress increases rapidly until the axial strain reaches 5% and then remains steady for a short time with increasing axial strain. When the axial strain is greater than 8%, the deviator stress decreases. Typical strain softening occurs in these samples.

3.2 Shear strength

Fig. 6 presents the shear strength of the tailings with a dipping interlayer. The red solid lines are the linear fitting curves of shear strength. The all slopes are negative, which indicates that the value of the curves decreases with increasing dip angle. Despite some observable scatter, there are reasons to believe that the shear strength decreases with increasing dip angle. Fig. 7 shows the relationship between the absolute value of the slope and the confining pressure. The absolute value of the slope exponentially increases with increasing confining pressure. It means that the weakened influence of confining pressure on shear strength is obviously.

3.3 Pore pressure

Fig. 8 presents the pore pressure curves of tailing specimens with dipping interlayers. The pore pressure curves increase in the form of an ‘S’. There is no negative pore pressure under high confining pressure. This indicates that contraction occurs only at the samples with interlayers. The dilation or contraction of the samples depends on the density of the sample and the confining pressure test

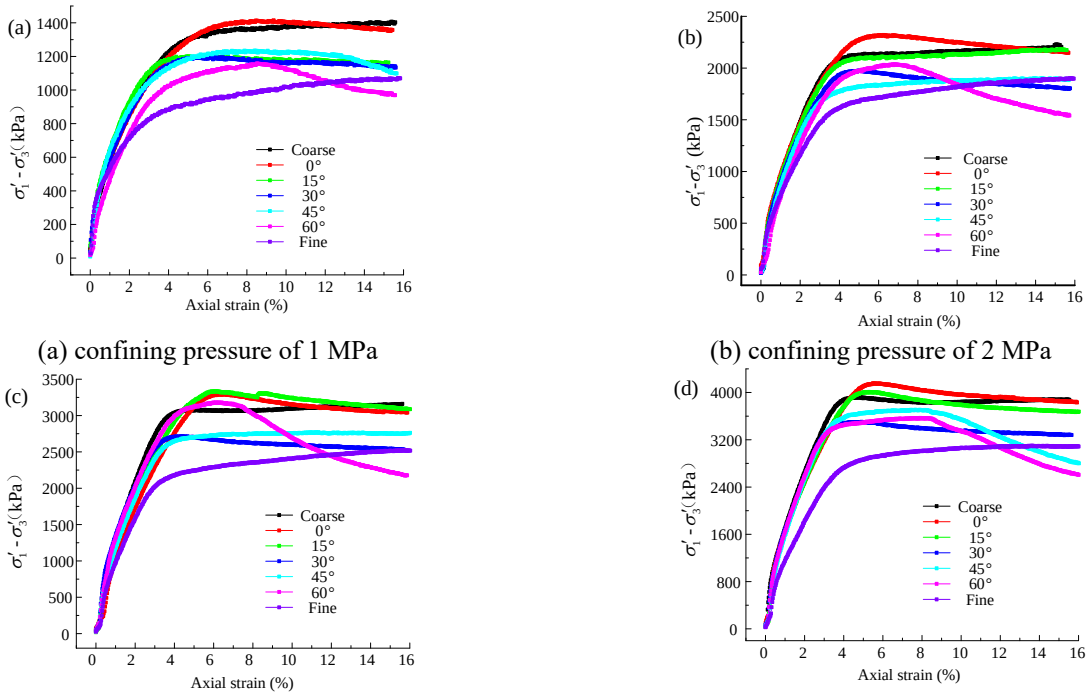

(a) confining pressure of 1 MPa

(b) confining pressure of 2 MPa

(c) confining pressure of 3 MPa

(d) confining pressure of 4 MPa

Fig. 5 stress-strain relationship curves of tailing specimens with dipping interlayer

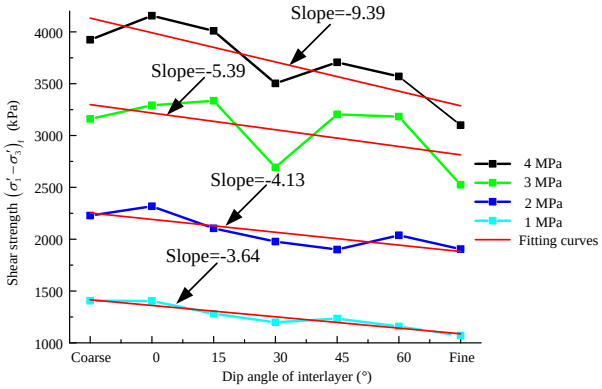

Fig. 6 Shear strength of tailing specimens with dipping interlayer

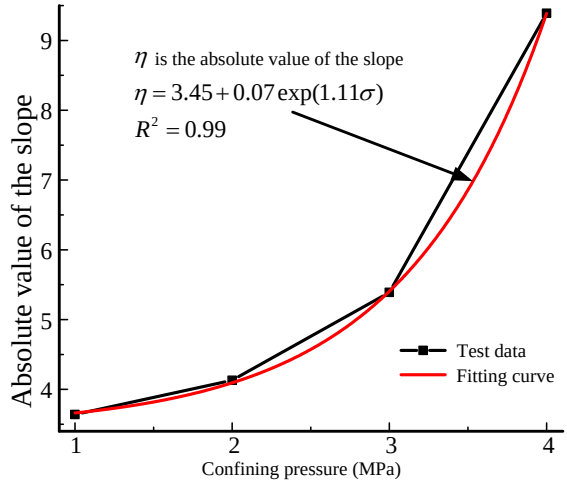

Fig. 7 Relationship between the absolute value of the slope and the confining pressure

(Bolton 1986). The contraction of the samples with an interlayer is completely dominated by the confining pressure when the confining pressure is high. This is attributed to the fact that the samples are in a normal consolidated state when the applied high confining pressure is high. The pore pressure of the sample increases very slightly until the axial strain reaches 2% and then increases rapidly, reaches a peak at an axial strain of 6%, and remains a certain constant value after the peak. It seems that there is a hysteresis effect in the increase in pore pressure. To clearly reveal the hysteresis effect, the pore pressure and stress-strain curves of samples with dipping interlayers at an angle of 30° under a confining pressure of 4 MPa are drawn in Fig. 9. The point where the stress increases rapidly is an axial strain of 0%. However, the point at which the pore pressure increases rapidly is the axial strain of 2.2%. This result is inconsistent with the conclusion that the pore pressure and stress both increase rapidly at an axial strain of 0% under low confining pressure (Keramatikerman and Chegenizadeh, 2017). Therefore, the hysteresis effect was verified. Moreover, a more interesting finding is that the maximal stress occurs at an axial strain of 4.4%, and the maximal pore pressure occurs at an axial strain of 7%. The pore pressure lags behind the stress by approximately 2-3% in axial strain from the overall perspective of the curve. The reason is that the elastic properties of the samples are large after consolidation under high confining pressure. The particle structure is more stable and can be subjected to external loading forces at the initial stage. Therefore, the particle pores are not filled. However, when the external loading forces reach a certain high level, the particle structure will be destroyed. The rapid decrease in particle pores causes a rapid increase in pore pressure.

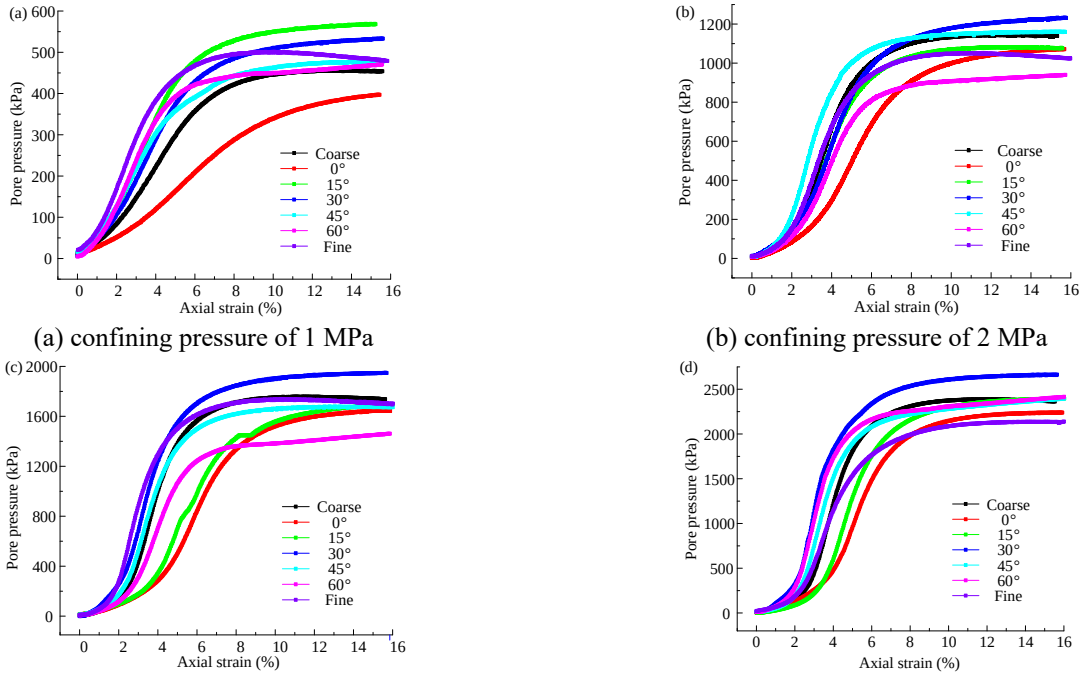

(a) confining pressure of 1 MPa (b) confining pressure of 2 MPa

(c) confining pressure of 3 MPa (d) confining pressure of 4 MPa

Fig. 8 Pore pressure curves of tailing specimens with dipping interlayer

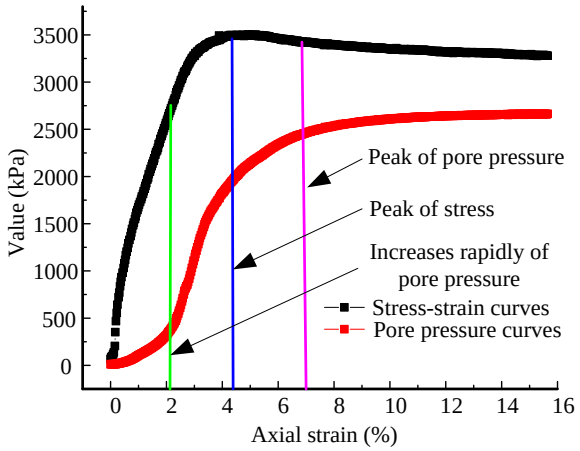

Fig. 9 Pore pressure and stress-strain curves of samples with dipping interlayer at angle of 30° under the confining pressure of 4 MPa

Fig. 10 presents the relationship between axial strain at the point of the rapid increase of pore pressure and the confining pressure. The axial strain at the point of the rapid increase of pore pressure increases with the increase of confining pressure. This indicates that the hysteresis effect of pore pressure is gradually obvious with increasing confining pressure and implies that the particle structure after consolidation is more stable with increasing confining pressure.

Fig. 11 presents the relationship between the peak pore pressure and the dip angle of the interlayer. The dipping interlayer has negligible effects on the peak pore pressure. The peak of the pore pressure of samples with an interlayer is nearly equivalent under the same confining pressure. In addition, the difference between the peak pore pressures of coarse and fine samples is small. This indicates that the influence of particle size on pore pressure is not obvious. Therefore, pore pressure is mainly affected by confining pressure under the high confining pressure.

3.4 Stress path

Fig. 12 presents the stress path curves of tailings with dipping interlayers in $p'-q$ space. $p'=(\sigma_1'+\sigma_3')/2$ is the mean effective stress, and $q=(\sigma_1'+\sigma_3')/2$ is the mean deviator stress. Except for the fine sample with a confining pressure less than 3 MPa, in which the stress path curves are 'S'-shaped, the stress path curves of the other samples are '7'-shaped. The stress paths of all samples with dipping interlayers are on top of the fine sample. Except for the samples with a dipping interlayer at an angle of 0° and the samples with a dipping interlayer at an angle of 15° under a confining pressure of greater than 3 MPa, the stress paths of other samples with a dipping interlayer are on the bottom of the coarse sample. This indicates that although the fine interlayer is capable of weakening the mechanical behaviour of the samples with interlayers, the mechanical behaviour of samples with dipping interlayers is still dominated by coarse tailings. Moreover, an obvious straight drop in the stress paths can be seen for samples with dipping interlayers at an angle of 60° after the peak. The straight line crosses the stress paths of the fine sample. The residual strength of the sample with a dipping interlayer at an angle of 60° is lower than that of the fine sample. The reason is that shear slipping occurred in the sample with a dipping interlayer at an angle of 60° and bulging deformation occurred in the fine sample, shown in Fig. 15.

The failure mechanism of shear slipping is different

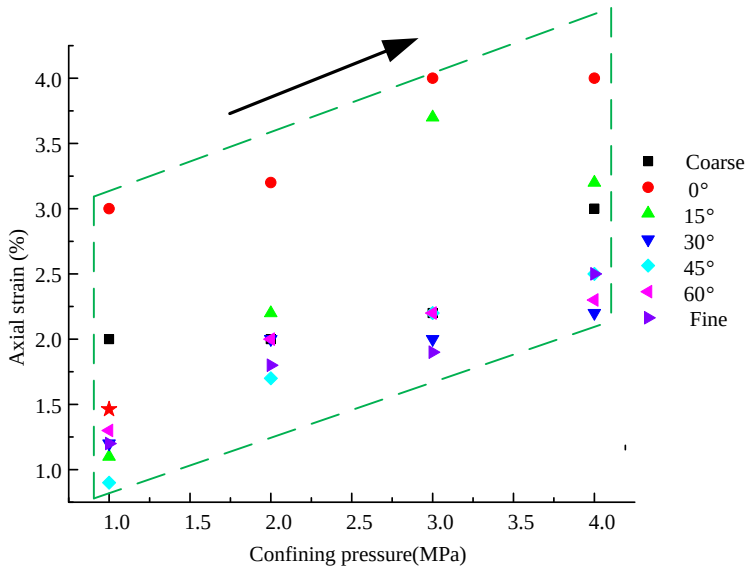

Fig. 10 Relationship between axial strain at the point of rapid increase of pore pressure and the confining pressure

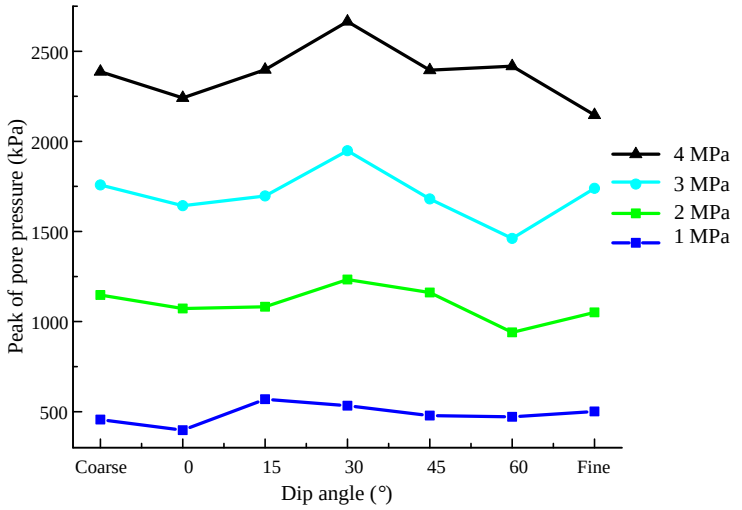

Fig. 11 Relationship between the peak of the pore pressure and the dip angle of the interlayer

from the bulging deformation. Once shear slipping failure is activated, the slipping surfaces will be misaligned with each other and reduce the contact area on the slipping surface. The mechanical behaviour of samples with interlayers will continue to deteriorate. This means that the dipping interlayer at a large angle tends to weaken the sample strength. The slopes of the straight line are less than 1 and decrease with increasing confining pressure. This indicates that the pore pressure increases with increasing confining pressure. Therefore, we should pay more attention when the angle of the dipping interlayer is large and the confining pressure is high.

3.5 Critical state line

The critical state line is the locus of void ratio-effective stress after shearing the soil samples to large displacement (Phan *et al.* 2016). This indicates that the samples are not affected by the drainage conditions and shearing modes.

The critical state line can be drawn by connecting the residual strength of each sample in a straight line in $p' = q$ space. Fig. 13 presents the critical state line of the tailings with dipping interlayers under high confining pressure. The slope of the critical state line of the samples with a dipping interlayer increases with increasing dip angle. The critical state lines of samples with dipping interlayers at angles of 0°, 15°, and 30° are close to those of the coarse samples, and the critical state lines of samples with dipping interlayers at angles of 45° and 60° are close to those of the fine samples. The critical state line of the sample with a dipping interlayer at an angle of 60° is below that of the fine sample, which is consistent with the findings that the stress path of the sample with a dipping interlayer at an angle of 60° crosses the stress paths of the fine sample. Although the shear strength of the sample with a dipping interlayer at an angle of 60° is larger than that of the fine sample, the residual strength of the sample with a dipping interlayer at an angle of 60° is less than that of the fine

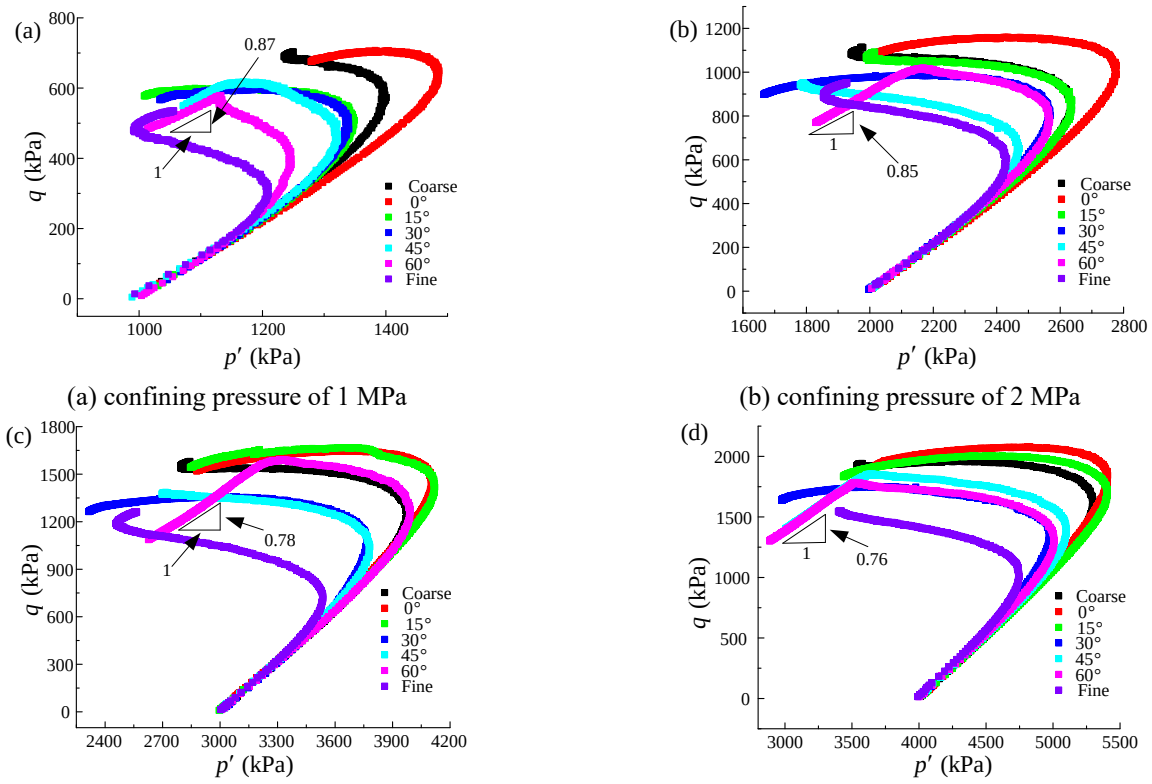

(a) confining pressure of 1 MPa (b) confining pressure of 2 MPa

(c) confining pressure of 3 MPa (d) confining pressure of 4 MPa

Fig. 12 Stress path curves of tailings with dipping interlayer

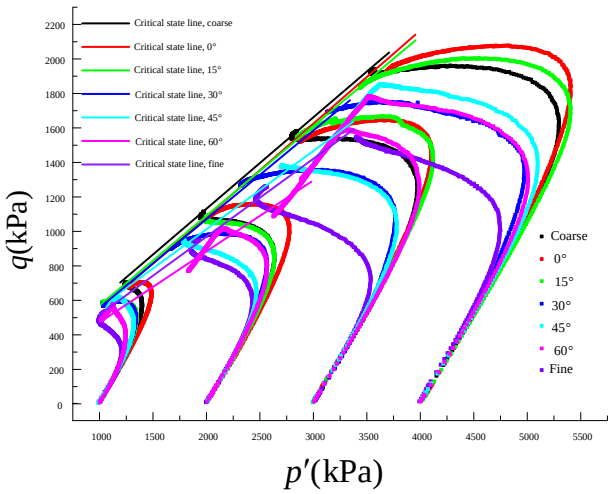

Fig. 13 Critical state line of the tailings with dipping interlayer

sample as long as shear slipping occurs along the weak interlayer. It means that the shear slipping along the interlayer has a great influence on the mechanical behaviour of the tailings samples. In fact, the formation of the potential sliding line is easily occurred along the weak surface when the tailing dams is failed. To prevent the disaster of a dam break, it is important to pay attention to the stability of the dam caused by weak interlayers when the angle between the interlayer plane and maximum principal stress plane is large.

The residual friction angle of the sample can be calculated from the slope of the critical state line. The equation is defined as

$$\varphi_c = \arcsin(M_c) \tag{1}$$

Fig. 14 presents the relationship between the residual friction angle and the angle of the dipping interlayer. The residual friction angle of the samples with a dipping interlayer decreases exponentially with the increasing angle of the dipping interlayer. The residual friction angle is in the range of 25°-34°. Except for the sample with a dipping interlayer at an angle of 60°, the residual friction angles of the other samples with a dipping interlayer are between

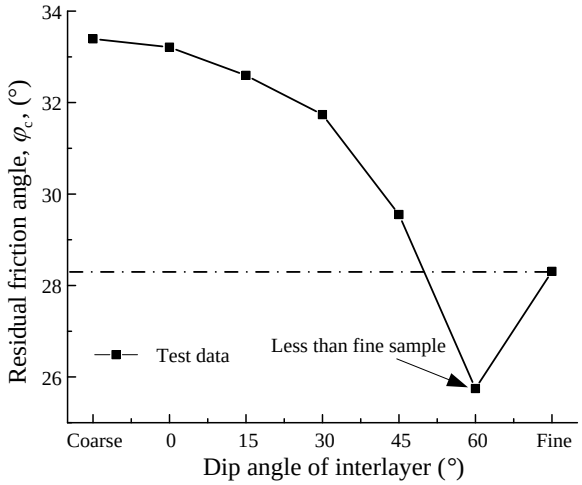

Fig. 14 Relationship between the residual friction angle and the dip angle of the interlayer

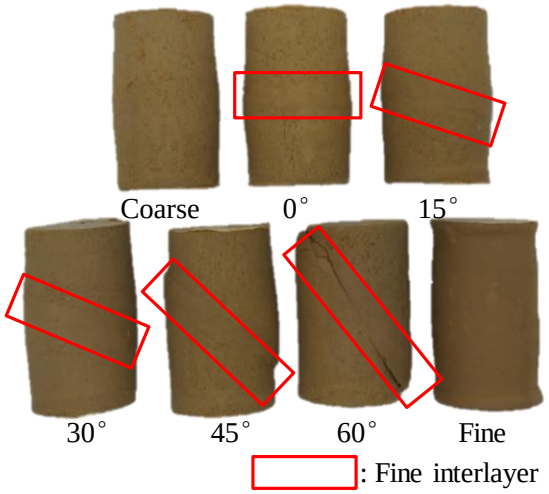

Fig. 15 Deformation patterns of tailings specimens

those of the coarse and fine samples. The residual friction angle of the sample with a dipping interlayer at an angle of 60° is lower than that of the fine sample. This indicates that the interlayer at a large dip angle has a great weakening effect on the mechanical behaviour of the sample with an interlayer.

3.6 Deformation properties

Fig. 15 shows the deformation properties of tailings with dipping interlayers under high confining pressure. The deformation patterns in the samples are as follows.

For the samples with dipping interlayers at angles of 0°, 15°, and 30°, with the coarse samples and the fine samples, the deformation at the middle part of the sample is obviously larger than that at the end part. Bulging deformation occurs in these samples. This means that the effect of the dipping interlayer on the deformation properties is negligible when the angle of the dipping interlayer is small. The mechanical behaviour is controlled by the coarse tailing.

For the samples with a dipping interlayer at an angle of 60°, shear slipping occurs along the dipping interlayer. Typical strain softening occurs in these samples. The shear strength is lower than in other samples. This means that the effect of the dipping interlayer on the deformation properties is obvious when the angle of the dipping interlayer is larger. The mechanical behaviour is controlled by the fine tailing.

For the samples with a dipping interlayer at an angle of 45°, both shear slipping and bulging deformation occur in these samples. A composite failure type is observed for these samples. It may be the critical angle of deformation for tailings with dipping interlayers under high confining pressure. Therefore, the angle between the lenticle structures and the direction of the principal stress should be as less as 45° as possible when the lenticle structures in tailing dams is inevitable.

3.7 Comparison of results under high and low confining pressures

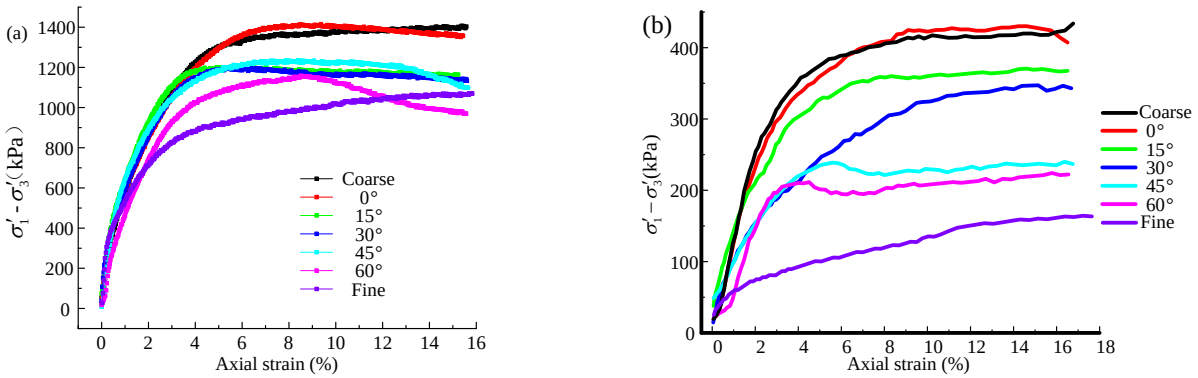

(a) high confining pressure of 1 MPa (b) low confining pressure of 100 kPa

Fig. 16 Comparison of stress-strain curves of samples with interlayer

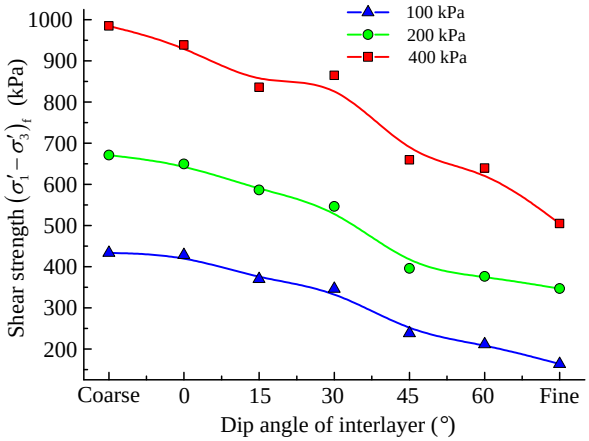

Fig. 17 Shear strength of samples with interlayer under low confining pressure

The mechanical properties of geomaterials under high confining pressure are different from those under low confining pressure. To clearly distinguish the differences caused by the confining pressure, the results in this paper are compared with those under low confining pressure. The results under low confining pressure are referenced in the literature of Chen *et al.* (2019).

3.7.1 Comparison of stress-strain curves under high and low confining pressures

To compare with the stress-strain curve under high and low confining pressures, the stress-strain curves of samples with dipping interlayers under a high confining pressure of 1 MPa and under a low confining pressure of 100 kPa are comparatively analyzed. Fig. 16 presents the comparison of stress-strain curves. For the samples with dipping interlayers at angles of 0°, 15°, and 30°, the tendencies of the stress-strain curves under high and low confining pressures are consistent. The stress increases rapidly with increasing axial strain and then remains at a certain value after reaching the peak. However, for the samples with dipping interlayers at angles of 45° and 60°, there are obvious differences in the stress-strain curves. For the samples with dipping interlayers at angles of 45°, the stress-strain curve maintains a certain value after the peak under high confining pressure. The stress-strain curve displays a slight stress drop after the peak and then maintains a certain value under low confining pressure. The reason may be that the lateral deformation of samples is restricted under high confining pressure. For the samples with dipping interlayers at angles of 60°, a continuous stress drop after the peak occurs under high confining pressure. The stress-strain curve displays a slight stress drop after the peak and then maintains a certain value under low confining pressure. It is similar to the samples with a dipping interlayer at an angle of 45° under low confining pressure. We can conclude that the stress-strain curves of samples with dipping interlayers at large angles under low confining pressure maintains a constant value after the stress drop. The stress will continuously decrease for tailings with dipping interlayers at large angles under high confining pressure. It indicates that the tailings material became brittle when the confining pressure was large and that the instability hazards of the high tailings dam were larger than those of the low tailings dam.

3.7.2 Comparison of shear strengths under high and low confining pressures

Fig. 17 presents the shear strength of samples with dipping interlayers under low confining pressures. Compare with Fig. 6, the tendency of shear strength under high confining pressure is similar to that under low confining

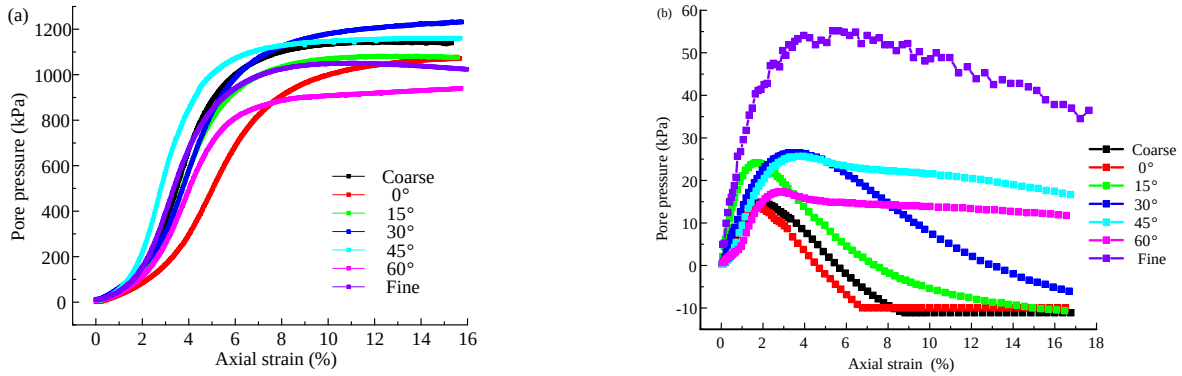

(a) high confining pressure of 2 MPa (b) low confining pressure of 100 kPa

Fig. 18 Comparison of the pore pressure curve

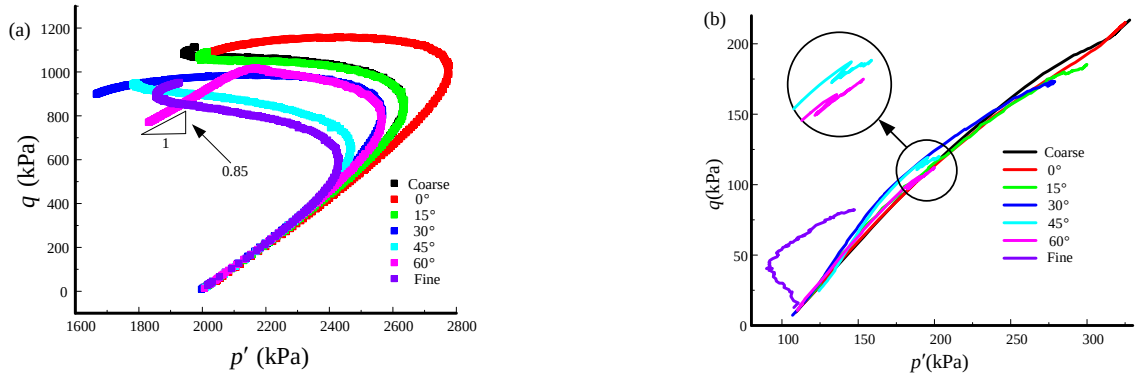

(a) high confining pressure of 2 MPa (b) low confining pressure of 100 kPa

Fig. 19 Comparison of the stress paths

pressure. The shear strength decreases with the increasing dip angle of the interlayer. This means that the weakening effect of the dipping interlayer on the samples is dominated by the dip angle of the interlayer and is not limited by the confining pressures.

3.7.3 Comparison of pore pressures under high and low confining pressures

To compare the pore pressure under high and low confining pressures, the pore pressure curves of samples with interlayers under a high confining pressure of 2 MPa and under a low confining pressure of 100 kPa are comparatively analyzed. Fig. 18 presents a comparison of the pore pressure curves. The evolution of pore pressure under high and low confining pressures is different. The pore pressure curves of all samples under high confining pressure are concentrated and show an 'S'. The positive pore pressure occurred in samples. The corresponding axial strain of the rapid increase of pore pressure is 2%, which indicates hysteresis effect. The reason is that the particle pores of the samples have difficulty decreasing after consolidation under high confining pressure during the small axial strain stage, because of the particle structure of the samples after consolidation under high confining pressure is more stable than that of the samples under low confining pressure.

All pore pressure curves under low confining pressure are scattered. The pore pressure curve of the fine sample obviously deviates from the other curves. The evolution of the pore pressure curves of the coarse samples and samples with dipping interlayers at angles of 0°, 15°, and 30° are the same. The pore pressure of these curves rapidly declines after the peak, and a negative pore pressure occurs. The evolution of the pore pressure curves of the samples with dipping interlayers at angles of 45° and 60° are the same. The pore pressure slightly drops after the peak and then maintains a certain value.

3.7.4 Comparison of stress paths under high and low confining pressures

To compare stress paths under high and low confining pressures, the stress path curves of samples with interlayers under a high confining pressure of 2 MPa and under a low confining pressure of 100 kPa are comparatively analyzed. Fig. 19 presents the comparison of the stress path curves. The tendency of the stress path under high and low confining pressures is different. The stress path of samples with an interlayer is in the form of a '7' under high confining pressure. Overlap does not occur in the stress path curves. The stress path of samples with an interlayer displays a linear relationship under low confining pressure. We can conclude that the stress paths of all samples with dipping interlayers are related to the coarse samples. It means that the thickness of the interlayer in this paper is rational. The mechanical behaviour of the samples with dipping interlayers is not affected by the thickness of the

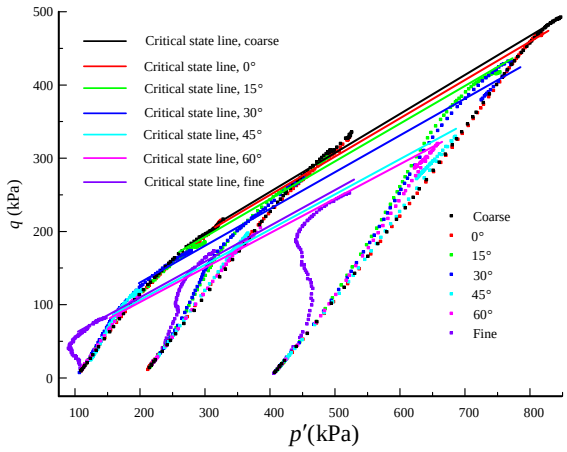

Fig. 20 Critical state line under low confining pressure

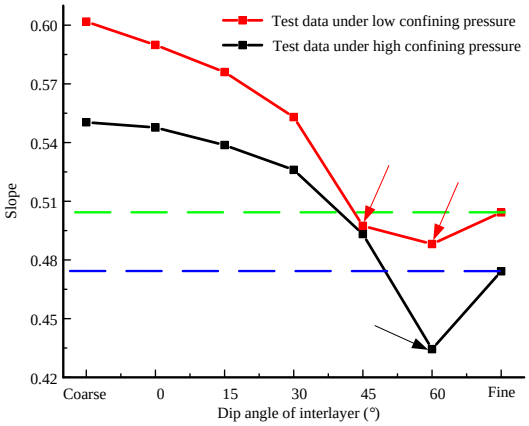

Fig. 21 Slope of the critical state line under high and low confining pressure

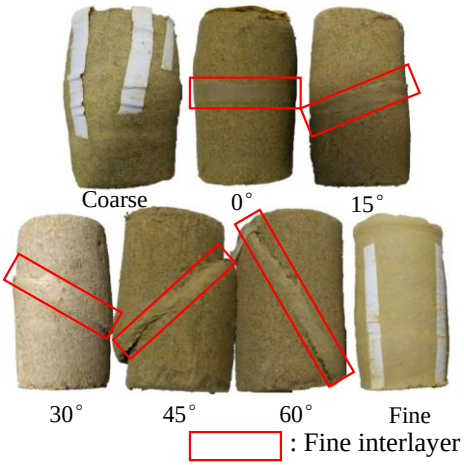

Fig. 22 Deformation of samples under low confining pressure

interlayer. Moreover, the stress path of the fine sample under low confining pressure and high confining pressure is in the form of an "L" and an "S", respectively. The reason is that the pore pressure of fine samples under high confining pressure slightly increases at the initial stage because a large amount of water is drained after consolidation.

3.7.5 Comparison of critical state lines under high and low confining pressures

Fig. 20 presents the critical state lines under low confining pressures. Compare with Fig. 13, the critical state line of the samples with dipping interlayers at small angles is close to that of the coarse sample, and at large angles is close to that of the fine sample. The critical state lines of samples with interlayers under high confining pressure are more scattered than those of samples with interlayers under low confining pressure. The critical state line under low confining pressure presents a bipolar distribution. The all critical state lines of the sample with an interlayer is below the coarse sample. For samples with dipping interlayers at angles of 45° and 60° under low confining pressure and the sample with a dipping interlayer at an angle of 60° under high confining pressure, the critical state lines are below the fine sample. The critical state lines of other samples are above the fine sample. Because the critical state line is a straight line passing through the origin, the relative position of the critical state line can be characterized by the slope of the critical state line (Li and Baudet 2016). Fig. 21 presents the slope of the critical state line of the samples under high and low confining pressures. The critical state line of the sample with a dipping interlayer at an angle of 60° is below that of the pure fine sample under high confining pressure. When the confining pressure is low, the critical state lines of the samples with dipping interlayers at angles of 45° and 60° are below those of the pure fine sample. The reason is that the residual strength caused by the shear slipping of the interlayer is lower than the residual strength caused by the bulging deformation. The slope of the sample with a dipping interlayer at an angle of 45° is larger than that of fine samples under high confining pressure. The reason is that shear slipping is difficult to occur because the lateral deformation is restricted under high confining pressure. This is consistent with the fact that rock samples exhibit strain hardening under high confining pressure (Li and Ma 2017). The slope of critical state line under high confining pressure is smaller than that of samples under low confining pressure. This implies that there is a nonlinear relationship between residual strength and confining pressure.

3.7.6 Comparison of deformation properties under high and low confining pressures

Fig. 22 presents the deformation of samples under low confining pressures. Compare with Fig. 15, the bulging deformation occurs in the samples with dipping interlayers at angles of 0° and 15° under low confining pressure and in the samples with interlayers dipping at angles of 0°, 15°, and 30° under high confining pressure. Shear slipping occurs in the samples with dipping interlayers at angles of 45° and 60° under low confining pressure and in the samples with dipping interlayers at an angle of 60° under high confining pressure. Composite deformation occurs in the samples with a dipping interlayer at an angle of 30° under low confining pressure and in the samples with a dipping interlayer at an angle of 45° under high confining pressure. Moreover, the deformation of the fine and course

samples is bulging deformation. There are three differences in the deformation for these samples. (1) The tailing sample under high confining pressure is compacted more densely than the tailing sample under low confining pressure. The hardness of the tailing samples under high confining pressure is larger than that of the samples under low confining pressure. (2) The deformation of the samples with a dipping interlayer at an angle of 30° is bulging deformation under high confining pressure. (3) The deformation of the samples with a dipping interlayer at an angle of 45° is composite deformation under high confining pressure due to the fact that the lateral deformation of samples is restricted under high confining pressure.

4. Discussion

For the actual tailings dams, some lenticles were inserted in the dam. The composition of the lenticles is fine tailings, i.e., clay and silt. Compared with coarse tailings, the mechanical behaviour of fine tailings is poor. Moreover, the permeability of fine tailings is lower than that of coarse tailings (Dong *et al*. 2021). Therefore, the risk of tailings dams with lenticle instability is increased. Particularly, when the angle between the direction of the principal stress and the distribution plane of the lenticle structures is near 60°, dam failure is prone to occur along the plane of the lenticles. Although the appearance of lenticles is inevitable (Morton 2021), the distribution and shape of lenticles is adjusted by the improved tailings slurry discharge method. The stability of the tailings dam may be improved by decentralized tailings slurry discharge.

According to the experimental results, the stress level is also weakened the shear strength of tailings. Although the hardness of the tailing samples under high confining pressure is larger than that of the samples under low confining pressure, other adverse factors occurred under the high pressure, such as the brittle behavior, the low residual friction angle and the positive pore pressure. Therefore, the instability hazards of high tailings dams are larger than those of low tailings dams. Four reasons can be summarized as follows:

(1) The storage capacity of high tailings dams is large. The gravitational potential energy increases with the storage capacity of tailings dams. Therefore, the risk of stability is also increases with the tailings slurry discharge. Once high tailings dam fails, a large amount of tailings flows downstream. The farmland and infrastructure downstream of the tailings dam are seriously threatened because of the submerged area is large. This makes us even more worried.

(2) The stress decreases continuously when shear slip occurs in the tailings sample. Once tailings dam with some lenticles failure occurs in the form of shear slip, the stress resistance decreases continuously due to the fact the stress continuously decreases after peak under high confining pressure. The tailings material became brittle. Thus, most tailings in dam ponds will be activated and flowed downstream. The risk of geological disasters is persistent for high tailings dams. Therefore, the instability hazards of the high tailings dam were larger than those of the low tailings dam.

(3) A positive pore pressure occurs, which reduces the effective stress. According to the effective stress principle, the effective stress is defined as follows

$$\sigma' = \sigma - u \tag{2}$$

where σ is the total stress and u is the pore pressure. The positive pore pressure occurred in samples under high confining pressure. The failure principle of the tailings dam is insufficient in effective stress. When enormous pore water pressure occurs under high stress level, the effective stress in tailing particles decreases, which increases the high tailings dam instability risk.

(4) The residual strength under high confining pressure is smaller than that under low confining pressure. The residual strength is the final strength that is approximately stable after the peak on the stress-strain curve of the soil. For high tailings dam, the residual strength is less than that of low dams. The distance of flowed tailings in high tailings dams is larger than that in low tailings dams due to low shear resistance. Moreover, considering the large storage capacity of the high tailings dam, the disaster of high tailings dam failure increases further.

5. Conclusions

This paper studies strength and deformation of tailings with fine-grained interlayers under high confining pressure. Consolidated undrained (CU) triaxial shear tests were carried out. The results in this paper were compared with results under low confining pressure. The main conclusions are as follows:

- Strain softening occurred in the samples with dipping interlayers at an angle of 60° under high confining pressure. The shear strength of the samples with an interlayer decreases with the increasing dipping interlayer angle. An obvious straight drop in the stress path after the peak occurs in samples with dipping interlayers at an angle of 60°. The critical state line of the sample with a dipping interlayer at an angle of 60° is below that of the fine sample. The results reveal that the mechanical behaviour of tailings with dipping interlayers is very sensitive to the angle of the interlayer under high confining pressure, especially for the sample with a dipping interlayer at an angle of 60°.
- Compared to the results under the low confining pressure, the stress-strain relationship of the samples with dipping interlayers at an angle of 45° is typical strain hardening under high confining pressure. Composite deformation occurred in the samples with dipping interlayers at an angle of 45° under high confining pressure. This reveals that the lateral deformation of the sample with an interlayer is seriously restricted by the confining pressure under a high confining pressure.
- The stress path of samples with an interlayer is in the form of a ‘7’ under high confining pressure. The stress path of samples with dipping interlayers under low confining pressure displays a linear relationship. The critical state lines of the sample with a dipping interlayer at

an angle of 60° under high confining pressure and the sample with a dipping interlayer at angles of 45° and 60° under high confining pressure are below that of the fine sample. The failures of these samples all display shear slipping. This indicates that the shear slipping along the interlayer in the samples seriously weakens the behaviour of tailings with the interlayer.

To improve the stability of the tailings dam, the decentralized tailings slurry discharge methods which is able to reduce the appearance of the lenticle structures can be adopted. Moreover, the shear strength parameters are change with increase of depth. Therefore, the zoning calculation method can be used for stability calculations of high tailings dams. The relationship between stress level and depth is worth studying. The nonlinear mechanical behavior of tailings should also be studied under high confining pressure.

Acknowledgments

The research was supported by the National Key Research and Development Program of China (NO. 2017YFC0804601). National Natural Science Foundation of China (No. 52104085).

References

Achterberg, E.P., Braungardt, C., Morley, N.H., Elbaz-Poulichet, F. and Leblanc, M. (1999), "Impact of Los Frailes mine spill on riverine, estuarine and coastal waters in southern Spain", *Water Res.*, **33**, 0-3394. https://doi.org/10.1016/s0043-1354(99)00282-1.

Azam, S. and Li, Q. (2010), "Tailings dam failures: a review of the last one hundred years", *Geotechnical news*, **28**, 50-54.

Blight, G.E. (1994), The master profile for hydraulic fill tailings beaches", *Geotech. Eng.*, **107**, 27-40. https://doi.org/10.1680/igeng.1994.25718.

Bolton, M.D. (1986), "The strength and dilatancy of sands", *Geotechnique*, **36**, 65-78. https://doi.org/10.1680/geot.1986.36.1.65.

Campbell, D.L. and Fitterman, D.V. (2000), "Geoelectrical methods for investigating mine dumps", *Proceedings of the 5th International Conference on Acid Rock Drainage (ICARD 2000)*, Denver, Colo, 1513-1523. Citeseer.

Cao, S., Xue, G.L., Yilmaz, E., Yin, Z.Y. and Yang, F.D. (2021), "Utilizing concrete pillars as an environmental mining practice in underground mines", *J. Cleaner Production*, **278**, 123433. https://doi.org/10.1016/j.jclepro.2020.123433.

Cao, S., Zheng, D., Yilmaz, E., Yin, Z.Y., Xue, G.L. and Yang, F.D. (2020), "Strength development and microstructure characteristics of artificial concrete pillar considering fiber type and content effects", *Constr. Build. Mater.*, **256**, 119408. https://doi.org/10.1016/j.conbuildmat.2020.119408.

Chen, Q.L., Zhang C., Yang C.H., Ma C.K., Pan Z.K. and Daemen, J.J.K. (2019), "Strength and deformation of tailings with fine-grained interlayers", *Eng. Geol.*, **256**, 110-120. https://doi.org/10.1016/j.enggeo.2019.04.007.

Cionek, V.M., Alves, G.H.Z., Tófoli, R.M., Rodrigues-Filho, J.L. and Dias, R.M. (2019), "Brazil in the mud again: lessons not learned from Mariana dam collapse", *Biodivers. Conserv.*, **28**(7), 1935-1938.

Davies, M.P. and Martin, T.E. (2000), "Upstream constructed tailings dams-a review of the basics", In Tailings and mine waste '00. *In Proceedings of the 7th international conference*, 3-15. Fort Collins.

Dong, L.Z., Deng, S.J. and Wang, F.Y. (2020), "Some developments and new insights for environmental sustainability and disaster control of tailings dam", *J. Cleaner Production*, **269**(10), 1-39. https://doi.org/10.1016/j.jclepro.2020.122270.

Dong, T., Cao, P., Gui, R., Lin, Q.B. and Liu, Z. (2021), "Experimental study on permeability coefficient in layered rine tailings under seepage condition", *Geofluids*, 1-14. https://doi.org/10.1155/2021/8850138.

Fan, X.S. and Masliyah. J. (1990), "Laboratory investigation of beach profiles in tailings disposal", *J. Hydraulic Eng.*, **116**, 1357-1373. https://doi.org/10.1061/(ASCE)0733-429(1990)116:11 (1357).

Farshad, R. (2011), "Tailings disposal options study for sangan iron mine project", *Proceedings of the Tailings and Mine Waste*, Iran.

GB/T50123 (1999), Standard for soil test method, Chinese.

Gomes, L.E.D.O., Correa, L.B., Sá, F., Neto, R.R. and Bernardino, A.F. (2017), "The impacts of the Samarco mine tailing spill on the Rio Doce estuary, Eastern Brazil", *Mar. Pollut. Bull.*, **120**, 28-36. https://doi.org/10.1016/j.marpolbul.2017.04.056.

Jeyapalan, J.K. (1982), "Dam-break studies for mine tailings impoundments", *Proceedings of the 5th Symposium on Uranium Mill Tailngs Managemem*. Fort Collins.

Jiang, H.Q., Han, J., Li, Y.H., Yilmaz, E., Sun, Q. and Liu, J. (2020), "Relationship between ultrasonic pulse velocity and uniaxial compressive strength for cemented paste backfill with alkali-activated slag", *Nondestructive Test. Eval.*, **35**(4), 359-377. https://doi.org/10.1080/10589759. 2019.1679140.

Jiang, W. D. (2005), "Fractal character of lenticles and its influence on sediment state in tailings dam", *J. Central South Univ. Technol. (English Edition)*, **12**, 753-756. https://doi.org/10.1007/s11771-005-0082-1.

Keramatikerman, M. and Chegenizadeh, A. (2017), "Effect of particle shape on monotonic liquefaction: Natural and crushed sand", *Exp. Mech.*, **57**, 1341-1348. https://doi.org/10.1007/s11340-017-0313-z.

Komnitsas, K., Kontopoulos, A., Lazar, I. and Cambridge, M. (1998), "Risk assessment and proposed remedial actions in coastal tailings disposal sites in Romania", *Miner. Eng.*, **11**, 1179-1190. https://doi.org/10.1016/S0892-6875(98)00104-6.

Koppe, J.C. (2021), "Lessons learned from the two major tailings dam accidents in Brazil", *Mine Water Environ.*, **40**(1), 166-173. https://doi.org/10.1007/s10230-020-00722-6.

Kou, Y.P., Jiang, H.Q., Ren, L., Yilmaz, E. and Li, Y.H. (2020), "Rheological properties of cemented paste backfill with alkali-activated slag", *Minerals*, **10**(3), 288. https://doi.org/10.3390/min10030288.

Krause, A.J. (1997), "Regulatory and technical tailings design considerations in Chile", *Proceedings of the International Conference on Tailings and Mine Waste'97*, Fort Collins.

Li, P.Q. and Baudet, B.A. (2016), "Strain rate dependence of the critical state line of reconstituted clays", *Géotechnique Lett.*, **6**, 66-71. https://doi.org/10.1680/jgele.15.00140.

Li, W. and Coop, M.R. (2018), "The mechanical behaviour of Panzhihua Iron tailings", *Can. Geotech. J.*, **56**, 420-435. https://doi.org/10.1139/cgj-2018-0032.

Li, X.B., Jiang, W.D. and He, H.J. (2004), "Study on distributing state of lenticle in tailings fill dam", *Rock Soils Mech.*, **25**, 947-949. https://en.cnki.com.cn/Article_en/CJFDTotal-YTLX200406028.htm.

Li, Y. L. and Ma, Z.Y. (2017), "A damaged constitutive model for rock under dynamic and high stress state", *Shock Vib.*, 1-6. https://doi.org/10.1155/2017/8329545.

Lottermoser, B.G. and Ashley, P.M. (2005), "Tailings dam seepage

at the rehabilitated Mary Kathleen uranium mine, Australia", *J. Geochem. Exploration*, **85**(3), 119-137. https://doi.org/10.1016/j.gexplo.2005.01.001.

Lumbroso, D., Davison, M., Body, R. and Petkovšek, G. (2021), "Modelling the Brumadinho tailings dam failure, the subsequent loss of life and how it could have been reduced", *Nat. Hazard. Earth Sys.*, **21**(1), 21-37. https://doi.org/10.5194/nhess-21-21-2021.

Ma, C.K., Zhang, C., Chen, Q.L., Pan, Z.K. and Ma, L. (2021), "On the effect of void ratio and particle breakage on saturated hydraulic conductivity of tailing materials", *Geomech. Eng.*, **25**(2), 159-170. https://doi.org/10.12989/gae.2021.25.2.159.

Martin, T. and McRoberts, E. (1999), "Some considerations in the stability analysis of upstream tailings dams", *Proceedings of the 6th International Conference on Tailings and Mine Waste*, 287-302. AA Balkema Rotterdam, Netherlands.

Moolman, P.L. and Vietti, A. (2012), "Tailings disposal: an approach to optimize water and energy efficiency", *The Southern African Institute of Mining and Metallurgy*, 767-779.

Morton, K.L. (2021), "The use of accurate pore pressure monitoring for risk reduction in tailings dams", *Mine Water Environ.*, **40**(1), 42-49. https://doi.org/10.1007/s10230-020-00736-0.

Özer, A.T. and Bromwell, L.G. (2012), "Stability assessment of an earth dam on silt/clay tailings foundation: a case study", *Eng. Geol.*, **151**, 89-99. https://doi.org/10.1016/j.enggeo.2012.09.011.

Pan, Z., Zhang, C., Li, Y. and Yang, C. (2022), "Solidification/stabilization of gold ore tailings powder using sustainable waste-based composite geopolymer", *Eng. Geol.*, 106793. https://doi.org/10.1016/j.enggeo.2022.106793.

Phan, V.T., Hsiao, D. and Nguyen, P.T. (2016), "Critical state line and state parameter of sand-fines mixtures", *Procedia Eng.*, **142**, 299-306. https://doi.org/10.1016/j.proeng.2016.02.045.

Shao, L., Chen, Z., Guo, X., Tian, X., Sun, Y., Hong, Z. and Jiang, W. (2021), "Hydraulic classification and sedimentation behaviors of iron tailings", *Bull. Eng. Geol. Environ.*, **80**(5), 3989-4000. https://doi.org/10.1007/s10064-021-02129-1.

Wang, G.J., Tian, S., Hu, B., Kong, X.Y. and Chen, J. (2020), "An experimental study on tailings deposition characteristics and variation of tailings dam saturation line", *Geomech. Eng.*, **23**(1), 85-92. https://doi.org/10.12989/gae.2020.23.1.085.

Wood, F.M., Yamamuro J.A. and Lade, P.V. (2008), "Effect of depositional method on the undrained response of silty sand", *Can. Geotech. J.*, **45**, 1525-1537. https://doi.org/10.1139/T08-079.

Wu, S.W., Yang, C.H., Zhang, C., Mao, H. and Li, H.R. (2016), "Microscopic geometric characteristics of surface sedimentary tailings", *Chinese J. Rock Mech. Eng.*, **35**, 768-777.

Xue, G. and Yilmaz, E. (2022), "Strength, acoustic, and fractal behavior of fiber reinforced cemented tailings backfill subjected to triaxial compression loads", *Constr. Build. Mater.*, **338**, 127667. https://doi.org/10.1016/j.conbuildmat.2022.127667.

Yin, G.Z., Li, G.Z., Wei, Z.A., Wan, L., Shui, G.H. and Jing, X.F. (2011), "Stability analysis of a copper tailings dam via laboratory model tests: A Chinese case study", *Miner. Eng.*, **24**, 122-130. https://doi.org/10.1016/j.mineng.2010.10.014.

Yin, G.Z., Wei, Z.A., Wang, J.G., Wan, G. and Shen, L.L. (2008), "Interaction characteristics of geosynthetics with fine tailings in pullout test", *Geosynthetics Int.*, **15**, 428-436. https://doi.org/10.1680/gein.2008.15.6.428.

Zhang, C., Chen, Q.L., Pan, Z.K. and Ma, C.K. (2020), "Mechanical behavior and particle breakage of tailings under high confining pressure", *Eng. Geol.*, **265**, 1-11. https://doi.org/10.1016/j.enggeo.2019.105419.

CC